



CHORUS

This is the accepted manuscript made available via CHORUS. The article has been published as:

Comprehensive Model for Randomly Phase-Matched Frequency Conversion in Zinc-Blende Polycrystals and Experimental Results for ZnSe

Taiki Kawamori, Qitian Ru, and Konstantin L. Vodopyanov

Phys. Rev. Applied **11**, 054015 — Published 6 May 2019

DOI: [10.1103/PhysRevApplied.11.054015](https://doi.org/10.1103/PhysRevApplied.11.054015)

Comprehensive Model for Randomly Phase-Matched Frequency Conversion in Zinc-Blende Polycrystals and Experimental Results for ZnSe

Taiki Kawamori, Qitian Ru, and Konstantin L. Vodopyanov

CREOL, College of Optics and Photonics, University of Central Florida, Orlando, Florida 32816, USA

(Dated: April 16, 2019)

Second-order nonlinear interactions in disordered materials based on random phase matching suggest intriguing opportunities for extremely broadband frequency conversion. Here we present a quantitative realistic model for random phase matching in zinc-blende polycrystals (ZnSe, ZnS, GaAs, GaP, etc.) that takes into account effects of random crystal orientation, grain size fluctuations, and includes polarization analysis of the generated output. Our simulations are based on rigorous transformation of the second-order susceptibility tensor in randomly rotated coordinates – to account for random orientation of crystalline domains, and demonstrate a good agreement with our experimental data for ZnSe using a nanosecond $\lambda = 4.7 \mu\text{m}$ source – in terms of variations of the strength and polarizations of the output fields. Also, it is revealed that random phase matching is most suitable for ultrafast (sub-100-fs) interactions with focused beams, e.g. second harmonic generation, sum and difference frequency generation, and optical parametric oscillation, that typically require short ($< 1 \text{ mm}$) interaction lengths, where disordered polycrystals can be on par, in terms of conversion yield, with ideal quasi phase matched crystals.

I. INTRODUCTION

Phase matching is a critical factor for generating new optical frequencies in the coherent process of nonlinear optical frequency conversion [1]. Birefringent crystals have been widely used to compensate phase mismatch, while quasi phase matching (QPM) is another technique to maintain growth of a new optical field by preventing destructive interference. An alternative approach is random phase matching (RPM) which avoids destructive interference by exploiting the random nature of disordered crystalline domains. A wide variety of materials can show this feature as long as they are composed of disordered microstructures possessing second-order nonlinear optical susceptibility. In the early stages of laser development, this has been used in a powder technique for evaluating nonlinear optical materials [2]. The first frequency conversion in a polycrystalline semiconductor where monocrystals are embedded with random orientations was demonstrated in 1966 and the variation of an output signal in terms of intensity and polarization has been qualitatively discussed [3]. Thanks to the fact that disordered polycrystalline materials have an extremely wide acceptance bandwidth they have been used as a nonlinear gain medium for a number of applications such as nonlinear optical microscopy, autocorrelation measurements, sum and difference frequency generation, and cascade harmonic generation [4–8].

In the field of ultrafast interactions, full advantage has been taken of the ultra-wide acceptance bandwidth associated with RPM: a spectrally broad high-average-power (0.3 W) second harmonic generation (SHG), and also a number of other wave mixing processes have been observed inside the gain media of mode-locked lasers based on Cr^{2+} -doped polycrystalline zinc sulfide (ZnS) and zinc selenide (ZnSe) samples [9, 10]. Most recently, an optical parametric oscillator (OPO) based on RPM was demonstrated in a ZnSe ceramic, pumped by femtosecond 2.35

μm laser pulses. The OPO produced an ultra-broad spectrum spanning 3–7.5 μm and exhibited a pump depletion as high as 79% [11]. Also, a multi-octave spectrum via simultaneous randomly phase matched three-wave mixing processes, facilitated by filamentation, was observed in polycrystalline ZnSe [12]. RPM can be viewed as an analogy of a random walk, where the electric field of the output wave grows as the square root of the interaction length within a nonlinear material. Mathematically, the main features of RPM in non-birefringent polycrystals with randomly oriented domains are the same as in the powder technique first outlined by Kurtz and Perry [2]. Namely, (1) the nonlinear conversion yield (in intensity) grows linearly with the sample thickness, (2) the highest conversion is achieved when the average grain size is close to the coherence length L_c , and (3) at a fixed sample length and optimized conditions, conversion efficiency is higher for larger coherence lengths. Although there were several attempts to analytically describe the frequency conversion process based on RPM [7, 8, 13, 14], none of them rigorously derived the probability distribution of the effective susceptibility of a randomly rotated crystal; also polarization analysis in RPM has been dismissed in these works. In this Letter, we present a model for ultrafast nonlinear $\chi^{(2)}$ interactions in an RPM material that includes random grain orientation, realistic grain size distribution, as well as variation of the two orthogonally polarized outputs due to the randomly transformed susceptibility tensor. We also calculate (for the first time to our knowledge) the efficiency of RPM process normalized to that of an ideal QPM process.

II. RANDOM SECOND-ORDER NONLINEAR SUSCEPTIBILITY

The three-wave mixing in $\chi^{(2)}$ media is characterized by the nonlinear polarization which is expressed as

$P_i^{(2)}(\omega) = \epsilon_0 \sum_{jk} \chi_{ijk}^{(2)}(\omega; \omega_1, \omega_2) E_j(\omega_1) E_k(\omega_2)$, where the indices refer to principal axis in a crystal coordinate system and $\chi_{ijk}^{(2)}$ is a second-order nonlinear optical susceptibility, which is a third-rank tensor. For zinc-blende semiconductors with a symmetry $\bar{4}3m$ it has six non-zero components for $i \neq j \neq k$ whose values are all the same under Kleinman symmetry. For the reason that three-wave mixing processes are reversible and are coupled through the same susceptibility tensor, the RPM analysis for the SHG efficiency is valid for its inverse process – subharmonic OPO [15]. Thus, we used the SHG process for both simulation and experiment, and the results are discussed later for the subharmonic femtosecond OPO generation.

The susceptibility variation in each successive grain was modeled by randomly rotated crystal coordinates (x, y, z) with respect to the laboratory frame (x', y', z') .

Here we describe it as three steps as shown in Fig. 1(a) after setting a random point $(x_0, y_0, z_0) = (\sin \theta \cos \phi, \sin \theta \sin \phi, \cos \theta)$ on a unit sphere in the laboratory frame, such that the probability density per unit surface area is uniform (see below). (1) Start with crystal's coordinate system that coincides with that of the laboratory frame. Rotate the crystal coordinate system by angle ϕ around z-axis (Fig. 1(a)). (2) Rotate the crystal coordinate system by angle θ around its new y-axis, so that the new z-axis directs to the point (x_0, y_0, z_0) . (3) Rotate the crystal coordinate system by random angle ψ (uniformly distributed between 0 to 2π) around the new z-axis. These operations are expressed in Eq. (1) as a product of three successive rotation matrices $R_{\vec{n}_1}(\phi)$, $R_{\vec{n}_2}(\theta)$ and $R_{\vec{n}_3}(\psi)$. Each matrix corresponds to a rotation by an angle ϕ, θ, ψ (Euler angles) about a fixed axis specified, respectively, by the unit vector defined as $\vec{n}_1 = (0, 0, 1)$, $\vec{n}_2 = (-\sin \phi, \cos \phi, 0)$ and $\vec{n}_3 = (x_0, y_0, z_0)$.

$$R = R_{\vec{n}_3}(\psi) R_{\vec{n}_2}(\theta) R_{\vec{n}_1}(\phi) = \begin{pmatrix} \cos \phi \cos \theta \cos \psi - \sin \phi \sin \psi & -\cos \phi \cos \theta \sin \psi - \cos \psi \sin \phi & \cos \phi \sin \theta \\ \cos \theta \cos \psi \sin \phi + \cos \phi \sin \psi & -\cos \theta \sin \phi \sin \psi + \cos \phi \cos \psi & \sin \phi \sin \theta \\ -\cos \psi \sin \theta & \sin \theta \sin \psi & \cos \theta \end{pmatrix} \quad (1)$$

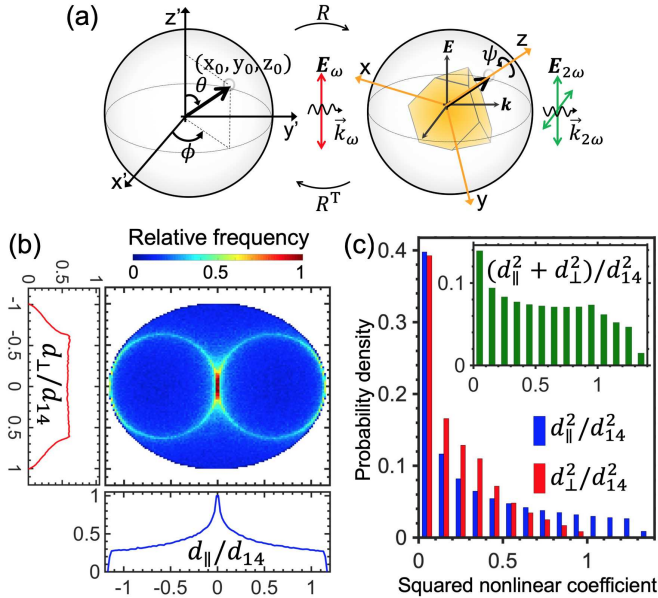


FIG. 1. (a) Schematic of the random rotation from a laboratory coordinate (x', y', z') to a crystal coordinate (x, y, z) and vice versa. (b) Correlation of the nonlinear coefficient in a randomly oriented single crystal between orthogonal polarizations and their projected 1D histograms. (c) Probability of the normalized squared nonlinear coefficient for parallel and perpendicular polarizations and their sum.

The nonlinear polarization in the laboratory frame is computed by the transformation rule for third-rank ten-

sors $\chi_{i'j'k'}^{(2)'} = R_{i'i}^T R_{j'j}^T R_{k'k}^T \chi_{ijk}^{(2)}$ [16]. In the contracted form, assuming the fundamental electric field is linearly polarized (parallel to z') and propagates along y' , the second-order polarization components that are parallel (along z') and perpendicular (along x') to the input polarization are given by

$$\begin{pmatrix} P_{\parallel}^{(2)'}(2\omega) \\ P_{\perp}^{(2)'}(2\omega) \end{pmatrix} = \epsilon_0 E^2(\omega) d_{14} \begin{pmatrix} 6R_{11}R_{21}R_{31} \\ 2R_{11}R_{21}R_{32} \\ +2R_{11}R_{22}R_{31} \\ +2R_{12}R_{21}R_{31} \end{pmatrix}. \quad (2)$$

We performed a Monte Carlo simulation of one million iterations for the nonlinear coefficient in a randomly oriented single crystal under the Euler angles' probability conditions of $\phi \in [0, 2\pi)$, $\theta = \arccos(u)$ where $u \in [-1, 1]$ and $\psi \in [0, 2\pi)$ [17]. These conditions ensure that the probability is uniformly distributed among all possible domain orientations in space. Fig. 1(b) shows the distribution of nonlinear coefficient for both parallel and perpendicular output polarizations in 1D and 2D color-coded form with respect to the linearly polarized incoming electric field. The nonlinear coefficient fluctuates within the expected range, $|d_{\parallel}/d_{14}| \leq \sqrt{4/3}$ for the parallel case, and $|d_{\perp}/d_{14}| \leq 1$ for the perpendicular case [18–20]. The correlation 2D map of Fig. 1(b) shows that numerous grains do not contribute to SHG, whereas there is a nonzero probability for the grains to align with the $[1\ 1\ 1]$ direction, which maximizes the nonlinearity and produces polarization contributing to the 'parallel' SH com-

ponent. Fig. 1(c) shows the distribution of the squared nonlinear coefficient, normalized to d_{14}^2 , – for parallel and perpendicular polarizations, and their combination (if no polarizer at the output is used). Table I shows the expected values of the modulus and the squared value of nonlinear coefficient. We note that the total (parallel plus perpendicular polarizations added) squared effective nonlinear coefficient is $0.57d_{14}^2$, which is substantially larger than the value $0.14d_{14}^2$ given in Ref. [7].

TABLE I. The expected value of the nonlinear coefficient in a randomly oriented single grain.

$ d_{ }/d_{14} $	$ d_{\perp}/d_{14} $	$d_{ }^2/d_{14}^2$	d_{\perp}^2/d_{14}^2	$(d_{ }^2 + d_{\perp}^2)/d_{14}^2$
0.48	0.41	0.34	0.23	0.57

III. EXPERIMENT AND RESULTS

The focus of our experimental study was ZnSe – a zincblende structure with a large coherence length, related to our specific application in ultrafast mid-infrared OPOs. First, we characterized the nonlinear optical properties of ZnSe ceramics through the SHG process (from 4.7 to 2.35 μm) using a nanosecond OPO source at $\lambda = 4.7$ μm (Fig. 2). The OPO was pumped by a $\lambda = 1.064$ μm Q-switched Nd:YAG laser with 20 ns pulse duration and 1.5 mJ pulse energy operating at 100 Hz repetition rate. The OPO linear cavity contained a fanned-out periodically poled lithium niobate (PPLN) crystal for frequency tuning, and produced a linearly polarized idler wave with an energy of about 15 μJ at 4.7 μm , which was focused at normal incidence into an RPM sample. The second harmonic output ($\lambda = 2.35$ μm) produced in a ZnSe ceramic sample was detected with an ‘extended’ InGaAs detector having a long-wave cutoff at 2.6 μm (thus it was ‘blind’ to the fundamental wave). A metal-grid polarizer was placed before the InGaAs detector to separately measure the two output SH polarizations. Our ZnSe samples were based on commercial CVD-grown ZnSe ceramics, where

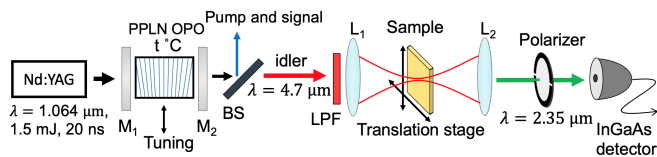


FIG. 2. Experimental setup for characterization of polycrystalline ZnSe via SHG. The PPLN OPO was tuned to select the idler wave of 4.7 μm . The beam splitter (BS) and the long-pass filter (LPF) rejected the OPO signal and the pump beams, and transmitted the OPO idler wave. The beam was focused by a $f = 50$ mm CaF₂ lens (L_1). A ZnSe sample was placed at the focus and scanned in x-y directions. The SH signal was collected by a $f = 50$ mm BK7 lens (L_2) and measured using an InGaAs detector.

the optimal average grain size was close to the coherence length (102 μm) of our studied nonlinear processes and was achieved by thermal annealing in vacuum at 900 $^{\circ}\text{C}$ [11]. The samples were cut and polished to a 5×10 mm cross section, and their thickness varied between 0.5 and 2 mm. The surface of a chemically etched sample revealing the grain structure is shown in Fig. 3(a).

To measure the grain size distribution we analyzed microscope etched surface images with the linear intercept method. The average grain size was 95 μm with a standard deviation of 48 μm . The distribution was best fitted with the lognormal function, as shown in Fig. 3(b). The samples were mounted on an XY translation stage, and the SH intensity for parallel and perpendicular polarizations was 2D mapped with 100- μm steps. The pump beam size was 50 μm (FWHM) and the depth of the focal region was longer than the crystal thickness.

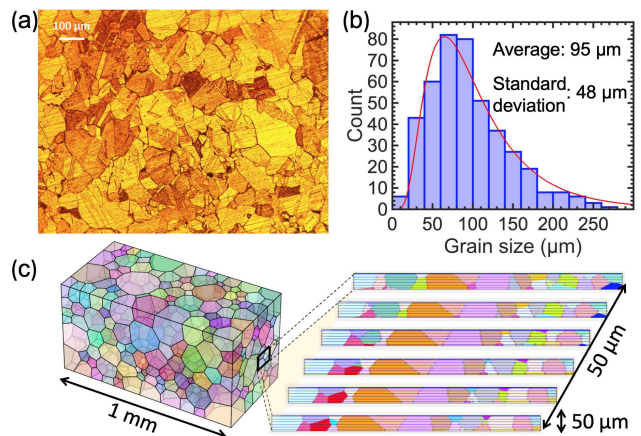


FIG. 3. (a) Cross section of a chemically etched ZnSe ceramic sample (total size 1.2×0.9 mm). (b) Histogram for the grain size distribution, which was measured by the line intercept method. Solid line – a lognormal fit. (c) A modeled polycrystalline structure created by Voronoi tessellation, where different colors correspond to different orientations of grains (left) and an example of a sliced $50 \mu\text{m} \times 50 \mu\text{m} \times 1$ mm structure that was used for $w \approx D$ simulation (right).

A typical mapping result for 1-mm-long sample (with the SH polarizations parallel and perpendicular to that of the pump) is shown in Fig. 4(a). One can see numerous ‘hot spots’, where the SH intensity is much higher than the average. These hot spots can be used for applications requiring high nonlinear gain. Fig. 4(b) plots the average SH power (parallel SH polarization) for different lengths of samples (which are all from the same origin). The linear dependence on the sample length confirms the prediction of the RPM theory [2]. The ratio of the average SH power for the parallel and perpendicular polarizations $P_{||}^{2\omega}/P_{\perp}^{2\omega}$ varied from 1.2 to 2.1 for different samples. Interestingly when the samples were rotated by 90° in the plane perpendicular to the beam, and the two measurements were averaged, the ratio became closer to 1.5, which is in accord with the simulated average value, as described below. The fact that the ratio $P_{||}^{2\omega}/P_{\perp}^{2\omega}$ was

not the same for different orientations indicates that the grain size and orientation are not purely random. The possible anisotropy can be due to a selected growth direction in the CVD process. The histograms of SH power for both output polarizations are shown in Fig. 4(c). (The normalizing factor was such that the average power for the parallel polarization is 1.)

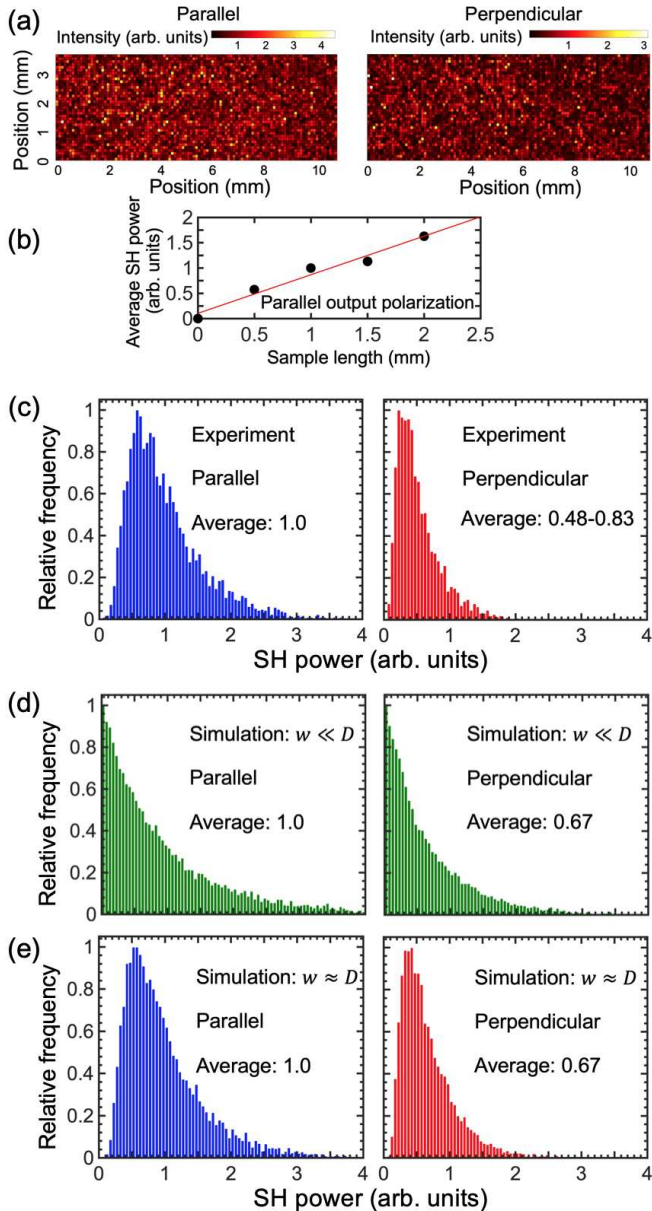


FIG. 4. (a) 2D color-coded plot for the relative SH power obtained by scanning a 1-mm-long sample with a 100- μm step for both parallel and perpendicular components. (b) Length dependence of the average SH power. (c) Histogram of SH power obtained from the mapping. The average values are 1.0 for parallel and 0.53 for perpendicular polarization, and their ratio is 1.9 in this case. (d,e) Simulated histograms of normalized SH power for the parallel and perpendicular components in the cases of $w \ll D$ and $w \approx D$.

IV. SIMULATIONS

RPM was numerically investigated for the two conditions in terms of the beam size w compared to the average grain size D . The model assumed the wave equation under the plane wave and non-depleted approximation, together with the derived random susceptibility tensor and real grain size distribution. Additionally, for analyzing the variation of second harmonic (SH) polarization through the randomly modified tensor, we regarded two orthogonally polarized output waves in the plane, transverse to the propagation direction [21]. First, we assumed that the beam size was much smaller than the average grain size, which is typically the case for high repetition rate ultrafast interactions. In this way, we performed 1D simulations along the beam propagation direction. The simulated histogram of Fig. 4(d) shows higher probability of weak SH signals, as compared to experiment (Fig. 4(c)). This mismatch comes from the fact that the beam inside the sample has a finite cross section and thus can ‘see’ several grains at a time. To analyze this effect, a polycrystalline structure model was created by Voronoi tessellation as shown in Fig. 3(c) [22]. It was based on a real ZnSe sample – in terms of distribution of the grain size and orientation. In this simulation, we assumed the real beam size (50 μm) and performed multiple 1D simulations with 10- μm steps in the transverse plane, assuming that the nonlinear polarizations induced in the neighboring grains (in the transverse plane) are uncorrelated. An example of 50 $\mu\text{m} \times 50 \mu\text{m} \times 1 \text{ mm}$ structure that was sliced into several cross sections along the beam propagation direction is shown in Fig. 3(c). The simulated SH power histogram that took into account averaging over the beam cross section, shown in Fig. 4(e), demonstrates a good agreement with experiment (Fig. 4(c)) – in terms of the histogram shape and the ratio $P_{\parallel}^{2\omega}/P_{\perp}^{2\omega}$. For large beams $w \gg D$, the variation of the output signal is expected to be even smaller due to the averaging effect in the transverse plane.

V. RANDOM-PHASE VS. QUASI-PHASE MATCHING

As predicted earlier [13] and demonstrated experimentally [9–12] RPM is very well suited for ultrafast three-wave interactions. In fact, the group-delay walk-off between the waves with different center wavelengths, especially when few-optical-cycle laser pulses are used, limits the interaction length to less than 1 mm. Using Monte Carlo simulations, we evaluated performance of RPM ZnSe for $w \ll D$ by comparing it with QPM. We modeled an ‘ideal’ ZnSe QPM material which uses nonlinear coefficient of $\sqrt{4/3}d_{14}$ (beam propagates along [1 1 0], all polarizations are along [1 1 1], by analogy with GaAs [19]). Fig. 5 shows RPM SHG efficiency for different sample lengths, normalized to that of an ‘ideal’ QPM crystal of the same length. One can see that the RPM vs.

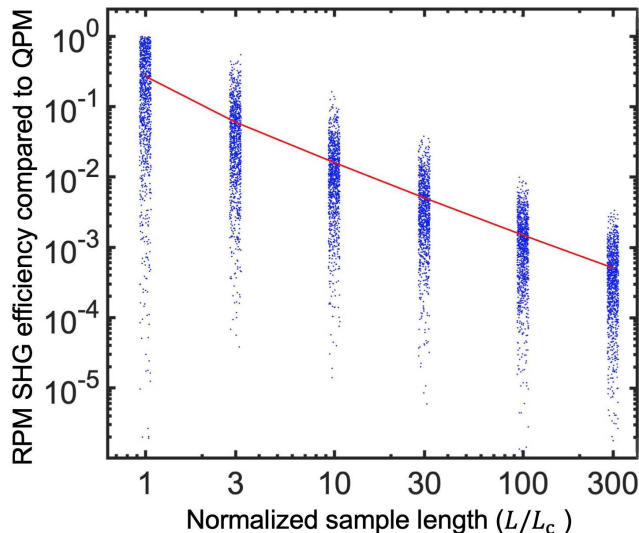


FIG. 5. RPM SHG efficiency for tightly focused beams normalized to that of an ideal QPM material (only parallel output component is counted) as a function of the normalized sample length. For each sample length (1, 3, 10, 30, 100, $300L_c$) the Monte Carlo simulation was performed using 1,000 sets of random structures and the average efficiency is shown as a solid line. Nonlinear coefficient of $\sqrt{4/3}d_{14}$ was used for the QPM condition.

QPM efficiency quickly degrades with the sample length (as $1/L$), however for shorter interaction lengths, there is a greater chance that RPM can perform on par with QPM. For example, at $L < 5L_c$, SHG efficiency in RPM hot spots can reach 50% of that of an ideal QPM crystal. This is totally consistent with the measured pump threshold in the femtosecond OPO that was based on RPM ZnSe and pumped at $\lambda = 2.35 \mu\text{m}$, demonstrated in [11]. Given the effective length for nonlinear inter-

action of $\sim 500 \mu\text{m}$ (5 ZnSe grains), determined by the depth of the focal region of the focused pump beam, and assuming $d_{14} \approx 20 \text{ pm/V}$ for ZnSe, we estimate that the 90-mW OPO pump threshold observed in the experiment was less than 2 times of that for an ideal QPM case.

VI. CONCLUSION

We have developed a rigorous model for RPM in a zinc-blende structure, which takes into account realistic distribution of the effective nonlinearity among the grains for both parallel and orthogonal output polarizations, as well as grain size distribution. We verified the model's predictions and found a good accord between experiment and theory. We have also shown that in the case of ultrafast interactions with focused beams, a disordered RPM material can perform on par with a QPM material. This is especially important for ZnSe, in which case QPM material is not yet available. Overall, RPM in polycrystalline materials opens a new route for ultrafast interactions, including frequency up and down conversion, as well as producing ultra-broadband mid-infrared OPO frequency combs.

ACKNOWLEDGMENTS

We are grateful to IPG Photonics – Mid-infrared Lasers for providing high-quality ZnSe polycrystalline samples. We also acknowledge the financial support from Office of Naval Research (ONR) (N00014-15-1-2659) and from Defense Advanced Research Projects Agency (DARPA) (W31P4Q-15-1-0008).

-
- [1] J. A. Armstrong, N. Bloembergen, J. Ducuing, and P. S. Pershan, Interactions between light waves in a nonlinear dielectric, *Phys. Rev.* **127**, 1918 (1962).
 - [2] S. K. Kurtz and T. T. Perry, A Powder Technique for the Evaluation of Nonlinear Optical Materials, *J. Appl. Phys.* **39**, 3798 (1968).
 - [3] C. K. N. Patel, Optical Harmonic Generation in the Infrared Using a CO₂ Laser, *Phys. Rev. Lett.* **16**, 613 (1966).
 - [4] R. Hellwarth and P. Christensen, Nonlinear optical microscopic examination of structure in polycrystalline ZnSe, *Opt. Commun.* **12**, 318 (1974).
 - [5] R. Kesselring, A. W. Kälin, and F. K. Kneubühl, Mid-Infrared Nonlinear Phenomena in Polycrystalline Semiconductors, *Appl. Phys. B* **55**, 437 (1992).
 - [6] T. D. Chinh, W. Seibt, and K. Siegbahn, Dot patterns from second-harmonic and sum-frequency generation in polycrystalline ZnSe, *J. Appl. Phys.* **90**, 2612 (2001).
 - [7] M. Baudrier-Raybaut, R. Haïdar, P. Kupecek, P. Lemasson, and E. Rosencher, Random quasi-phase-matching in bulk polycrystalline isotropic nonlinear materials, *Nature* **432**, 374 (2004).
 - [8] R. Kupfer, H. J. Quevedo, H. L. Smith, L. A. Lisi, G. Tiwari, C. G. Richmond, B. B. Bowers, L. Fang, and B. M. Hegelich, Cascade random-quasi-phase-matched harmonic generation in polycrystalline ZnSe, *J. Appl. Phys.* **124**, 243102 (2018).
 - [9] S. Vasilyev, I. Moskalev, M. Mirov, S. Mirov, and V. Gapontsev, Three optical cycle mid-IR Kerr-lens mode-locked polycrystalline Cr²⁺:ZnS laser, *Opt. Lett.* **40**, 5054 (2015).
 - [10] S. Vasilyev, I. Moskalev, V. Smolski, J. Peppers, M. Mirov, V. Fedorov, D. Martyshkin, S. Mirov, and V. Gapontsev, Octave-spanning Cr:ZnS femtosecond laser with intrinsic nonlinear interferometry, *Optica* **6**, 126 (2019).

- [11] Q. Ru, N. Lee, X. Chen, K. Zhong, G. Tsoy, M. Mirov, S. Vasilyev, S. B. Mirov, and K. L. Vodopyanov, Optical parametric oscillation in a random polycrystalline medium, *Optica* **4**, 617 (2017).
- [12] R. Šuminas, G. Tamošauskas, G. Valiulis, V. Jukna, A. Couaïron, and A. Dubietis, Multi-octave spanning nonlinear interactions induced by femtosecond filamentation in polycrystalline ZnSe, *Appl. Phys. Lett.* **110**, 241106 (2017).
- [13] E. Y. Morozov and A. S. Chirkin, Stochastic quasi-phase matching in nonlinear-optical crystals with an irregular domain structure, *Quantum Electron.* **34**, 227 (2004).
- [14] X. Vidal and J. Martorell, Generation of Light in Media with a Random Distribution of Nonlinear Domains, *Phys. Rev. Lett.* **97**, 013902 (2006).
- [15] R. W. Boyd, *Nonlinear optics*, 3rd ed. (Academic Press, 2008).
- [16] F. Zernike and J. E. Midwinter, *Applied Nonlinear Optics* (Wiley, New York, 1973).
- [17] G. Marsaglia, Choosing a Point from the Surface of a Sphere, *Ann. Math. Stat.* **43**, 645 (1972).
- [18] T. Skauli, K. L. Vodopyanov, T. J. Pinguet, A. Schober, O. Levi, L. A. Eyres, M. M. Fejer, J. S. Harris, B. Gerard, L. Becouarn, E. Lallier, and G. Arisholm, Measurement of the nonlinear coefficient of orientation-patterned GaAs and demonstration of highly efficient second-harmonic generation, *Opt. Lett.* **27**, 628 (2002).
- [19] K. L. Vodopyanov, O. Levi, P. S. Kuo, T. J. Pinguet, J. S. Harris, M. M. Fejer, B. Gerard, L. Becouarn, and E. Lallier, Optical parametric oscillation in quasi-phase-matched GaAs, *Opt. Lett.* **29**, 1912 (2004).
- [20] K. L. Vodopyanov, Polarization-insensitive nonlinear-optical devices, *Proc. SPIE* **6875**, 68750 (2008).
- [21] P. S. Kuo and M. M. Fejer, Mixing of polarization states in zincblende nonlinear optical crystals, *Opt. Express* **26**, 26971 (2018).
- [22] R. Quey, P. R. Dawson, and F. Barbe, Large-scale 3D random polycrystals for the finite element method: Generation, meshing and remeshing, *Comput. Methods Appl. Mech. Eng.* **200**, 1729 (2011).